Cyclopalladation of a Covalent Organic Framework for Near-Infrared Light-Driven Photocatalytic Hydrogen Peroxide Production

Andrés Rodríguez-Camargo,[a,b] Maxwell W. Terban,[a] Martina Paetsch,[a,b] Elio A. Rico,[c] Radhika Hirpara,[b] Viola Duppel,[a] Igor Moudrakovski,[a] Martin Etter,[c] Néstor Guijarro,[d] Robert E. Dinnebier,[a] Liang Yao*,[e] Bettina V. Lotsch*[a,b,f]

[a] Nanochemistry Department
Max Planck Institute for Solid State Research
Heisenbergstraße 1, 70569 Stuttgart, Germany
E-mail: b.lotsch@fkf.mpg.de

[b] Department of Chemistry
University of Stuttgart
Pfaffenwaldring 55, 70569 Stuttgart, Germany

[c] Deutsches Elektronen-Synchrotron (DESY)
Notkestrasse 85, Hamburg 22607, Germany

[d] Institute of Electrochemistry
University of Alicante
Apartat 99, E-03080 Alacant, Spain

[e] State Key Laboratory of Luminescent Materials and Devices, Institute of Polymer Optoelectronic Materials and Devices, Guangdong Basic Research Center of Excellence for Energy and Information Polymer Materials
South China University of Technology
Guangzhou 510640, P. R. China
Email: liangyao@scut.edu.cn

[f] Department of Chemistry
Ludwig-Maximilian University of Munich
Munich 81377, Germany

Abstract

Covalent organic frameworks (COFs) have been extensively developed as photosensitizers for photocatalytic energy conversion over the past decade. However, current COF photocatalysts have yet to demonstrate the capability to harvest near-infrared (NIR) light (above 760 nm), which constitutes approximately 53% of the solar spectrum, for fuel or chemical conversion. In this work, we introduce a novel post-synthetic functionalization strategy for COFs by incorporating a palladacycle directly into the COF backbone, extending the light absorption of an azobenzene-based COF into the NIR region. This approach enables homogeneous, atomically-distributed Pd functionalization with a high loading amount of 12 wt% and without noticeable formation of Pd nanoparticles. The cyclopalladated COF, TpAzo-CPd, was utilized as a catalyst for photocatalytic hydrogen peroxide production under 810 nm illumination. This study represents the first implementation of COFs for NIR photocatalysis and opens the door to Pd-single-site COF catalysts for a wide range of organic transformations.

Introduction

Since the first demonstration in 2005,[1] covalent organic frameworks (COFs) have emerged as a powerful platform for creating functional porous materials by covalently linking a variety of building blocks. The customizable molecular structures and functionalities of COFs offer promising routes to applications in diverse fields, such as gas storage and separation,[2,3] sensing,[4] water harvesting,[5,6] and drug delivery.[7,8] In 2014, our group demonstrated the use of COFs as light-harvesting materials for photocatalytic solar energy conversion, enabling the storage

of solar energy in the form of hydrogen fuel.[9] Subsequently, COFs have rapidly evolved as photocatalysts for solar energy conversion and are successfully employed in various reactions, including the reduction of CO_2,[10] the degradation of organic pollutants,[11] and the oxidative hydroxylation of arylboronic acids to produce phenols,[12] among others. Nevertheless, the photocatalytic reactions driven by COFs have so far been restricted to utilizing visible light (< 760 nm). Yet, there is a burgeoning interest in exploiting near-infrared light (NIR, > 760 nm) for photocatalytic applications, particularly given that NIR light comprises a substantial fraction of the solar spectrum, approximately 53%.[13] A significant challenge in extending the light responsivity of COF photocatalysts into the NIR region is the relatively low energy of NIR light, which provides limited driving force for photocatalytic reactions. Under these circumstances, it is crucial for NIR COF photocatalysts to possess mitigated charge recombination, enabling efficient utilization of the absorbed NIR photon energy to drive the chemical conversion reactions. Moreover, it is important to note that only a limited number of strategies have been reported to prepare COFs capable of harvesting NIR light, primarily involving the incorporation of building blocks with extended pi-conjugation or supporting intramolecular charge transfer .[14, 15] This limitation further complicates the search for suitable NIR COF photoabsorbers through material screening.

Over the past decade, post-synthetic modification of COFs has been established as an effective approach to enrich the diversity and functionality of COFs. Among the various post-synthetic modification strategies, the metalation of COFs has drawn an increasing attention in recent years in the field of photocatalysis, since this treatment has demonstrated to introduce active sites for targeted reactions.[16] In 1965, Cope *et al.* synthesized a cyclopalladated complex derived from azobenzene, documenting a pronounced red-shift in the optical characteristics.[17] Subsequent investigations have

further diversified the chemistry of azo-cyclopalladated compounds, resulting in a variety of derived structures.[18] These cyclopalladated complexes have exhibited remarkable catalytic performance across a range of reactions including C-C cross-coupling, reduction of aromatic nitro compounds, and C-H activation.[19] Nevertheless, despite the recognized utility of cyclopalladated complexes, to the best of our knowledge, their integration into COFs remains unexplored so far.

In the present study, we successfully applied cyclopalladation to an azo-based COF (TpAzo COF) following meticulous optimization of reaction conditions. We found that the utilization of methanol as the reaction solvent yields a highly functionalized cyclopalladated TpAzo COF (Figure 1). The resulting COF exhibits a uniform distribution of site-isolated palladium atoms without notable formation of palladium nanoparticles, thereby providing an effective solution to circumvent the formation of palladium nanoparticles—a significant synthetic challenge generally encountered in the integration of palladium complexes into COFs.[20, 21, 22] Cyclopalladation induces a significant broadening of the light absorption of the COF, thus shifting the absorption edge into the NIR region. Taking advantage of this NIR light-harvesting capability, we here introduce the first NIR light-harvesting COF photocatalyst for photocatalytic solar energy conversion, affording the production of H_2O_2, a widely used and valuable industrial chemical.

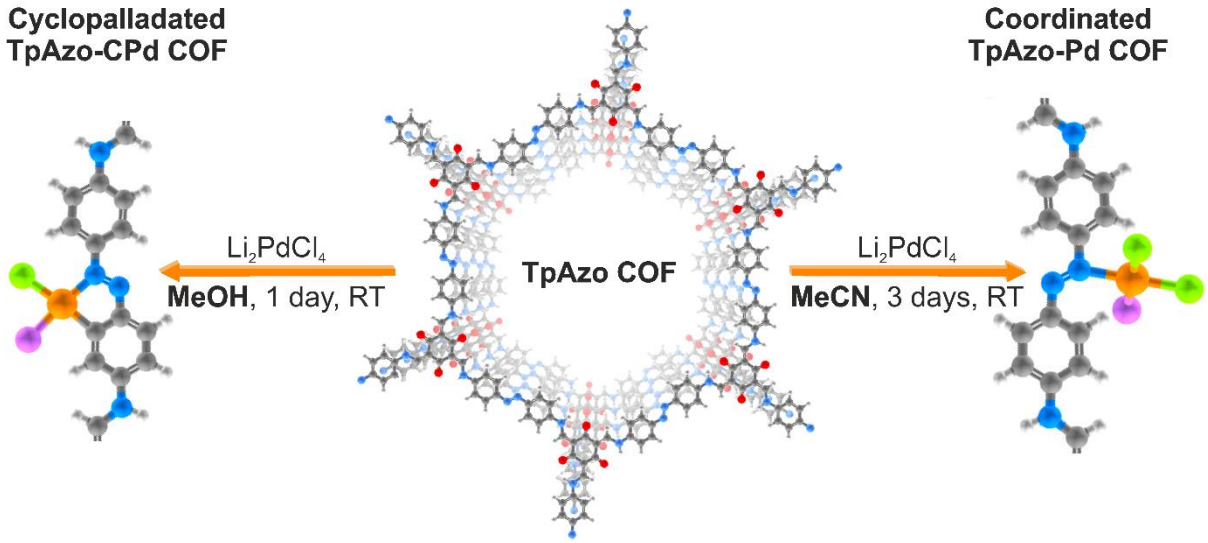

Figure 1. Schematic representation of TpAzo COF palladation obtained by the use of methanol and acetonitrile, respectively. In gray, carbon atoms; white, hydrogen; red, oxygen; blue, nitrogen; orange, palladium; green, chlorine and purple, the representation of exchangeable ligands.

Results and discussion

Cyclopalladation of TpAzo COF

In the cyclopalladation of an azobenzene derivative, the formation of the carbon-metal bond involves deprotonation of the phenyl ring, resulting in the generation of HCl as a byproduct when using Li_2PdCl_4. Since a number of COFs are sensitive to acidic conditions, β-ketoenamine was adopted as the COF linkage in this work and TpAzo COF was prepared *via* a solvothermal route. To enhance the crystallinity of TpAzo, pyrrolidine was utilized as reaction catalyst.[23] The cyclopalladation was performed using Li_2PdCl_4 as palladium source, prepared *in situ* from LiCl and $PdCl_2$. Li_2PdCl_4 solution was slowly added dropwise to a TpAzo COF dispersion under constant stirring to prevent palladium nanoparticle formation. Two reaction solvents,

MeOH and MeCN, were compared for the cyclopalladation reaction. We found that MeOH results in the formation of site-isolated cyclo-Pd complexes, while MeCN only provides coordinated Pd atoms (see details below). To simplify the discussion, the pristine TpAzo COF was designated as 'TpAzo', the COF post-palladation using MeCN as the solvent as 'TpAzo-Pd,' and the one using MeOH as the solvent as 'TpAzo-CPd'.

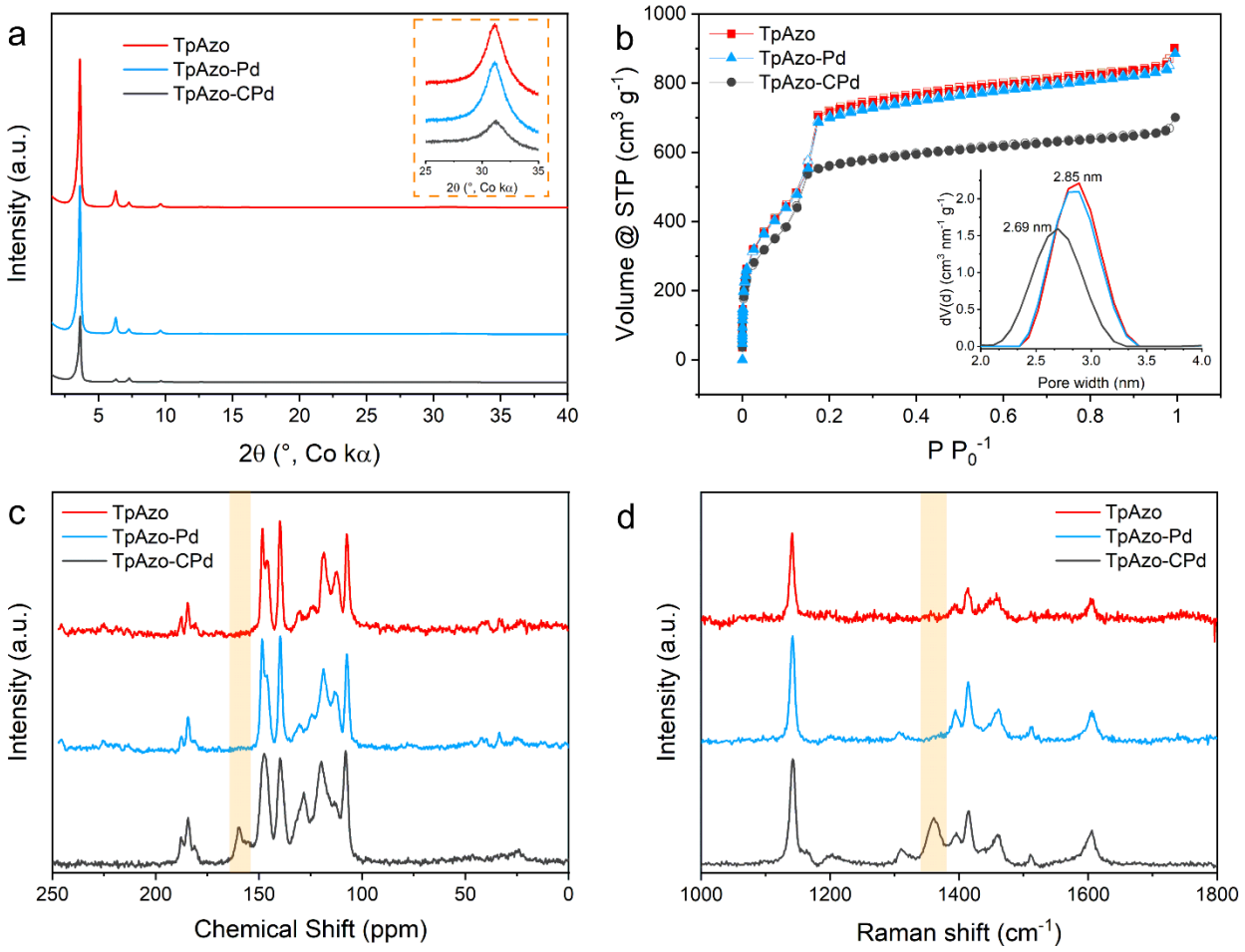

Figure 2. Structural characterization of TpAzo, TpAzo-Pd and TpAzo-CPd COFs. a) PXRD patterns. b) N_2 sorption isotherms and pore size distributions. c) ^{13}C solid-state NMR. d) Raman spectra after baseline correction.

After conducting the post-synthetic palladation on the pristine TpAzo, the amount of anchored palladium was quantified using inductively coupled plasma optical

emission spectroscopy (ICP-OES), giving a palladium amount of 2.76 ± 0.05 wt% for TpAzo-Pd and 12.60 ± 0.05 wt% for TpAzo-CPd (Table S1). TpAzo-CPd exhibits a palladium content four times higher than that of TpAzo-Pd, indicating that the coordination of Pd atoms to TpAzo COF likely varies depending on the solvent used. The crystallinity of the pristine COF and Pd functionalized COFs were studied by powder X-ray diffraction (PXRD) analysis. All three materials, namely TpAzo, TpAzo-Pd, and TpAzo-CPd, exhibit five distinct diffraction peaks (Figure 2a) at 2θ = 3.6°, 6.3°, 7.3°, 9.6°, and 31.1° (Co $K\alpha_1$ radiation), corresponding to the 100, 110, 200, 210, and 001 reflections, respectively.[24] This observation suggests that the COF structure is robust enough to retain the crystallinity under the acidic reaction conditions and during the incorporation of palladium ions into the framework. Interestingly, TpAzo-CPd does exhibit noticeable alterations in the relative intensity of the reflections at 6.3° and 7.3° 2θ, which will be discussed in more detail in the following section.

Next, the impact on COF porosity afforded by the incorporation of palladium into the framework was assessed by examining N_2 sorption isotherms (see Figure 2b). Both the pristine COF and the palladated COFs exhibit typical isotherms of mesoporous adsorbents, characterized by the distinct inflection in nitrogen uptake at low relative pressure (centered around 0.1 P P_0^{-1}).[25] The N_2 sorption isotherm for TpAzo-Pd closely resembles that of pristine TpAzo, while TpAzo-CPd exhibits a reduction in gas uptake, likely correlated with the substantial incorporation of the cyclo-Pd complex. TpAzo and TpAzo-Pd show very similar Brunauer-Emmett-Teller (BET) surface areas of 2077 $m^2\ g^{-1}$ and 2064 $m^2\ g^{-1}$, respectively, while the BET surface area of TpAzo-CPd is decreased to 1643 $m^2\ g^{-1}$. In addition, TpAzo and TpAzo-Pd share the same pore size of 2.85 nm. In comparison, TpAzo-CPd shows a pore size of 2.69 nm, slightly smaller than TpAzo and TpAzo-Pd (Figure

S5-S7). The above results demonstrate that the limited palladium functionalization in TpAzo-Pd has a minor impact on the porosity of TpAzo COF. In contrast, the decreased pore size and BET surface area of TpAzo-CPd can be rationalized by the substantial incorporation of palladium species into the pore walls of the framework.

Next, solid-state nuclear magnetic resonance (ssNMR) and Raman spectroscopy were conducted to confirm the success of cyclopalladation in TpAzo-CPd. As shown in Figure 2c, the ^{13}C-ssNMR of all the three samples show notable signals between 110 ppm and 140 ppm, and the signals around 180 ppm assigned to the carbonyl carbon in the keto form of the Tp moiety are present for all the samples. While the majority of signals remained unchanged after cyclo-Pd complex incorporation, a new peak centered at 159 ppm emerged for TpAzo-CPd. This can be attributed to the aromatic carbon directly bonded to palladium, as documented in reported literature, which establishes the formation of an organometallic bond through cyclopalladation (detailed assignment shown in Figure S8).[26, 27] In addition, 2D heteronuclear correlation NMR (^{1}H-^{13}C HETCOR-NMR) was performed to investigate the proton-carbon correlation in TpAzo-CPd (Figure S9). It can be seen that the carbon signal at 159 ppm shows no coupling with any proton, consistent with the nature of a C-Pd bond. Moreover, Figure 2c demonstrates that no obvious change in ^{13}C signals is observed between TpAzo-Pd and TpAzo, even after extending the reaction time to 10 days, indicating that no cyclopalladation takes place for TpAzo-Pd (Figure S10). Furthermore, ^{15}N-ssNMR was performed on TpAzo COFs containing ^{15}N-enriched Azo linker (details provided in SI). As displayed in Figure S12, TpAzo and TpAzo-Pd exhibit identical ^{15}N-ssNMR spectra, implying a largely unchanged chemical environment of nitrogen atoms in TpAzo-Pd. In contrast, TpAzo-CPd shows a noticeable shift in its spectrum, with the signal for the NH linkage shifted from -243 to -239 ppm and the signal for the azo nitrogen

atoms shifted from -20 ppm to -31 ppm for pristine TpAzo COF and TpAzo-CPd, respectively (Figure S12). The success of cyclo-Pd complex formation in TpAzo-CPd was also confirmed by Raman and Fourier-transform infrared spectroscopy (FT-IR). As displayed in Figure 2d and S16, the appearance of the peak centered at 1387 cm^{-1} in the Raman spectrum and distinct changes in the fingerprint region of the FT-IR spectrum around 1200 cm^{-1} are observed for TpAzo-CPd, which can be assigned to the vibrational modes pertaining to the bonding between carbon and palladium atoms in the cyclo-Pd complex.[28]

Putting the aforementioned structural characterization together, it can be inferred that C-Pd bonding is facilitated under conditions employing MeOH as the solvent, whereas the utilization of MeCN does not favor the formation of C-Pd bonding.[29] We rationalize the solvent effect by considering that MeOH (19.0 kcal mol^{-1}) has a higher donor number than MeCN (14.1 kcal mol^{-1}),[30] which may translate into a better proton accepting ability from azobenzene upon cyclopalladation (Figure S17).

Optical Properties

It is noted that an obvious change in the color of the COF powder is observed upon the incorporation of palladium into TpAzo COF (Figure 3a). Vis-NIR diffuse reflectance spectroscopy (Vis-NIR DRS) was employed to investigate the effect of metal coordination on the optical properties of COFs. The pristine TpAzo COF shows strong visible light absorption with an onset at 599 nm (Figure S18), resulting in a reddish-colored powder. When palladium was incorporated into the COF, a significant broadening of the absorption range is obtained: the absorption onset of TpAzo is red-shifted to 692 nm for TpAzo-Pd and 804 nm for TpAzo-CPd (Figure 3b, Figure S19 and S20). These results indicate that the cyclopalladation in TpAzo COF enables the extension of light absorption into the NIR region. The remarkable influence of palladium on the optical properties of TpAzo COFs likely arises from a

metal-to-ligand charge transfer (MLCT) transition, as commonly observed in cyclometallated complexes.[31, 32]

To confirm that the observed color change is due to palladium complexation, a couple of control experiments were conducted. First, it has been demonstrated that the protonation of the COF linkage in acidic media can cause a significant bathochromic shift in the absorption spectra.[33] To rule out this possibility, TpAzo COF was exposed to a methanolic solution of HCl at a concentration equivalent to the assumption that all moles of $PdCl_2$ used in the palladation synthesis were released as moles of protons in the form of HCl. This sample, referred to as TpAzo+HCl, exhibited an absorption spectrum almost identical to that of the pristine COF (Figure S24), thus disproving the notion that the broad light absorption of TpAzo-CPd is due to COF protonation.

Secondly, 4-dimethylaminoazobenzene, also known as methyl yellow (MY), was employed as a model molecule of TpAzo COF to evaluate the effect of cyclopalladation on optical properties, due to its structural similarity to the TpAzo fragment. Using the same palladation protocol, MY was successfully functionalized to MY-CPd (Figure S25). Notably, the light absorption spectra of these two samples exhibited a similar trend to that of TpAzo and TpAzo-CPd, where cyclopalladation extended the light absorption into the infrared region (*ca*. 100 nm shift on the absorption onset, Figure S26), confirming that the NIR light absorption of TpAzo-CPd originates from cyclo-Pd complexation.

In addition, a control COF containing benzidine rather than azobenzene (TpBz COF) was further synthesized and used to understand the crucial role of azobenzene on the optical property change after Pd incorporation. Since it has been reported that the ketoenamine linkage also coordinates with palladium ions,[20] using TpBz COF as a control system allows to verify whether the observed red-shift in absorption is

attributable to the coordination between the ketoenamine linkage and Pd ions. Following the same synthetic protocol used for TpAzo-CPd, Pd was incorporated into TpBz COF, designated as TpBz-Pd. The palladium content of TpBz-Pd was determined to be 3.10 ± 0.03 wt% by ICP-OES, which is very similar to TpAzo-Pd (2.76 ± 0.08 wt%). However, Vis-NIR DRS spectra reveal that only a minor red-shift is obtained for TpBz-Pd compared to pristine TpBz COF, clearly different from the pronounced red-shift in TpAzo-Pd and TpAzo-CPd (Figure 3c). This comparison suggests that the significant change in optical properties following Pd decoration is predominantly due to the coordination between Pd atom and azobenzene moiety, rather than the ketoenamine linkage. This result is consistent with the aforementioned structural characterizations, which identify azobenzene as the primary site of Pd atom coordination.

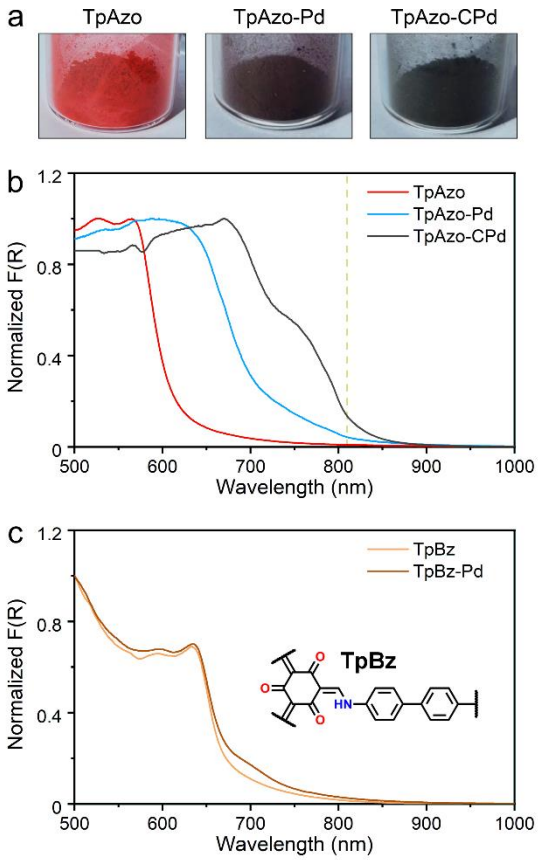

Figure 3. a) Photographs of the COF powders. b) Kubelka-Munk function from Vis-NIR diffuse reflectance spectra of TpAzo, TpAzo-Pd and TpAzo-CPd; vertical dashed green line indicates 810 nm. c) Kubelka-Munk function from Vis-NIR diffuse reflectance spectra of TpBz and TpBz-Pd; inset represents the chemical structure of TpBz COF.

Palladium environment in TpAzo-CPd COF

Having confirmed the presence of Pd-C bond formation and its optical properties, we next sought to more closely investigate the Pd coordination environment in TpAzo-CPd COF. First, to confirm the presence of chloride atoms in the COF structure, quantification of Cl was carried out by elemental analysis (Table S2), yielding a weight percentage of chloride of 6.22 wt%. Together with the Pd amount quantified by ICP-OES, the atomic ratio between Pd and chloride is estimated to be 1.42 (Table S2). The lower atomic ratio than 2 suggests the possible attachment of exchangeable ligands to the complex, such as water or methanol.[26, 29] Based on this information, we considered three different coordination scenarios to estimate the ratio of azo groups forming cyclopalladated complexes (Figure S29). The results indicate that approximately 60% of the azo groups in TpAzo-CPd are present as cyclopalladated complexes (Figure S29).

As the cyclopalladated azobenzene crystal structure (Azobenzene-CPd) reveals that cyclopalladation can lead to a contraction of the azobenzene moiety (Figure S30), subtle structural modifications can be expected in TpAzo-CPd COF after cyclopalladation. As depicted in Figure 4a-c and Figure S31, TpAzo-CPd shows a shift in the 100 (2θ of ~0.017°) and 001 reflections (2θ of ~0.128°) compared to TpAzo and TpAzo-Pd. This can be rationalized by the cyclopalladation resulting in a contraction of the Azo linker (Figure S30) as well as a slightly shortened π-π stacking distance, due to the distortion of the cyclopalladation complex. In addition,

Figure 4b shows a relative intensity change of the 110 and 200 reflections after cyclopalladation. Such a behavior is due to the addition of electron density to the COF pore in the form of -$PdCl_2$ (Figure S32).

To further investigate the Pd coordination environment in TpAzo-CPd, difference pair distribution function (dPDF) analysis was carried out.[34, 35, 36] As shown in Figure 4d, significant peaks in the dPDF between TpAzo-CPd and TpAzo can be observed, particularly at r = 2.3, 3.1, and between 4-6 Å, suggesting a coherent structure modification due to the presence of bound Pd complexes. It is noted that no major dPDF signals are obtained comparing TpAzo-Pd and TpAzo (Figure S33), further implying the negligible structural change when using acetonitrile as the reaction solvent. Moreover, the absence of the peaks assigned to the metallic Pd structure (Figure 4e), specifically the Pd-Pd distance at 2.7 Å, allows us to exclude the presence of Pd nanoparticles in TpAzo-CPd. As it has been reported that Pd(II) ions are easily transformed to Pd nanoparticles when synthesizing Pd functionalized COFs,[20, 21, 22] dPDF suggests that our synthesis affords a large amount of Pd(II) complex incorporation without noticeable formation of Pd nanoparticles. In addition, the single-crystal structure of cyclopalladated azobenzene compounds reveals a distortion in planarity by the formation of the palladacycle, driven by the steric effect of the coordinated ligands and the adjacent protons.[29] Therefore, we also considered the possibility of a planarity change by the introduction of the Pd complex. It can be seen that introducing a torsion angle of 30° between the two phenyl rings of the azobenzene (Figure 4e) results in a better match of the nearest neighbor Pd distance distribution, including Pd-C/N approx. 2.0 Å and Pd-Cl approx. 2.3 Å. Moreover, a better fit in the range of 3–6 Å is obtained for the non-planar model compared to the planar one. Combining the above results and other

simulations (Figure S34), it is inferred that a distortion of the TpAzo 2D framework is induced by the formation of the cyclopalladation complex (Figure 4f).

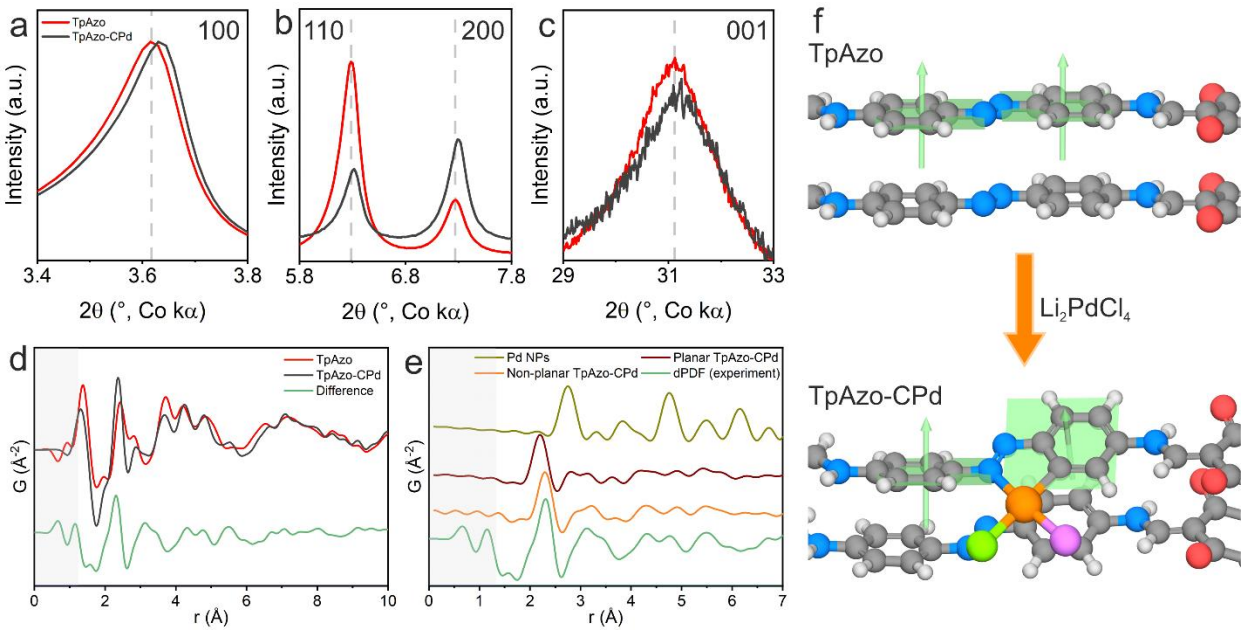

Figure 4. Comparison of 100 (a), 110 and 200 (b), and 001 (c) reflections of TpAzo and TpAzo-CPd PXRD patterns. d) PDF comparison of TpAzo-CPd and TpAzo, showing a significant modification in the local structure signal. The shaded grey area represents the low-r region most affected by systematic errors during the data processing. e) Comparison of dPDF signals calculated from different models. f) Scheme of proposed models of TpAzo and TpAzo-CPd. In gray, carbon atoms; white, hydrogen; red, oxygen; blue, nitrogen; orange, palladium; green, chlorine; purple, exchangeable ligands, and light green, representation of the plane described by the phenyl ring and its perpendicular vector.

Transmission electron microscopy (TEM), scanning electron microscopy (SEM) and X-ray photoelectron spectroscopy (XPS) were conducted to study the Pd site isolation and the Pd electronic environment in TpAzo-CPd, respectively. As shown in Figure 5a, TpAzo-CPd displays crystalline domains with a lattice spacing of 2.67 nm (Figure S38), attributed to the 100 reflection of TpAzo-CPd and matching well

with the distance obtained from the PXRD pattern. Additionally, a negligible quantity of Pd NPs was found as darker spots under TEM (Figure S39). Energy-dispersive X-ray spectroscopy coupled with scanning TEM (STEM-EDX) further suggests that palladium and chlorine are uniformly distributed and well-mixed with carbon in TpAzo-CPd, demonstrating homogeneous functionalization by cyclopalladation throughout the sample (Figure 5b). Indeed, SEM images confirm the absence of Pd nanoparticles in TpAzo-CPd across micrometer sized regions (Figure 5c). The SEM images collected using an energy-selective backscattered electron detector (ESB) and a type II secondary electron detector (SE2) show no evidence of visible bright dots indicative of Pd nanoparticles. The effectiveness of SEM-ESB/SE2 characterization is validated by measuring a control sample, obtained by treating TpAzo-CPd with $NaBH_4$, thereby reducing the Pd complex to Pd nanoparticles (denoted as TpAzo-CPd+$NaBH_4$). SEM-ESB images of TpAzo-CPd+$NaBH_4$ reveal numerous bright dots signaling the presence of a significant amount of Pd nanoparticles. Further characterizations of TpAzo-CPd+$NaBH_4$ by FT-IR, Kubelka-Munk function analysis and XPS additionally prove that the palladacycle is destroyed upon reduction (Figure S43, S44 and S45). In the Pd 3d XPS spectrum of TpAzo-CPd, two distinct peaks appear at 337.9 eV and 343.2 eV, corresponding to the $3d_{5/2}$ and $3d_{3/2}$ core levels of Pd(II) ions forming a chlorinated palladium complex (Figure 5d).[37, 38] In addition, the peaks at 198.4 eV and 200.0 eV are observed in the Cl 3p XPS spectrum, attributed to the $2p_{3/2}$ and $2p_{1/2}$ core levels of a chloride species (see Figure 5d).[39] These results provide compelling evidence that the palladium in TpAzo-CPd mainly exists as isolated Pd(II) sites in the form of cyclopalladation complexes with chloride ions as the ligand.

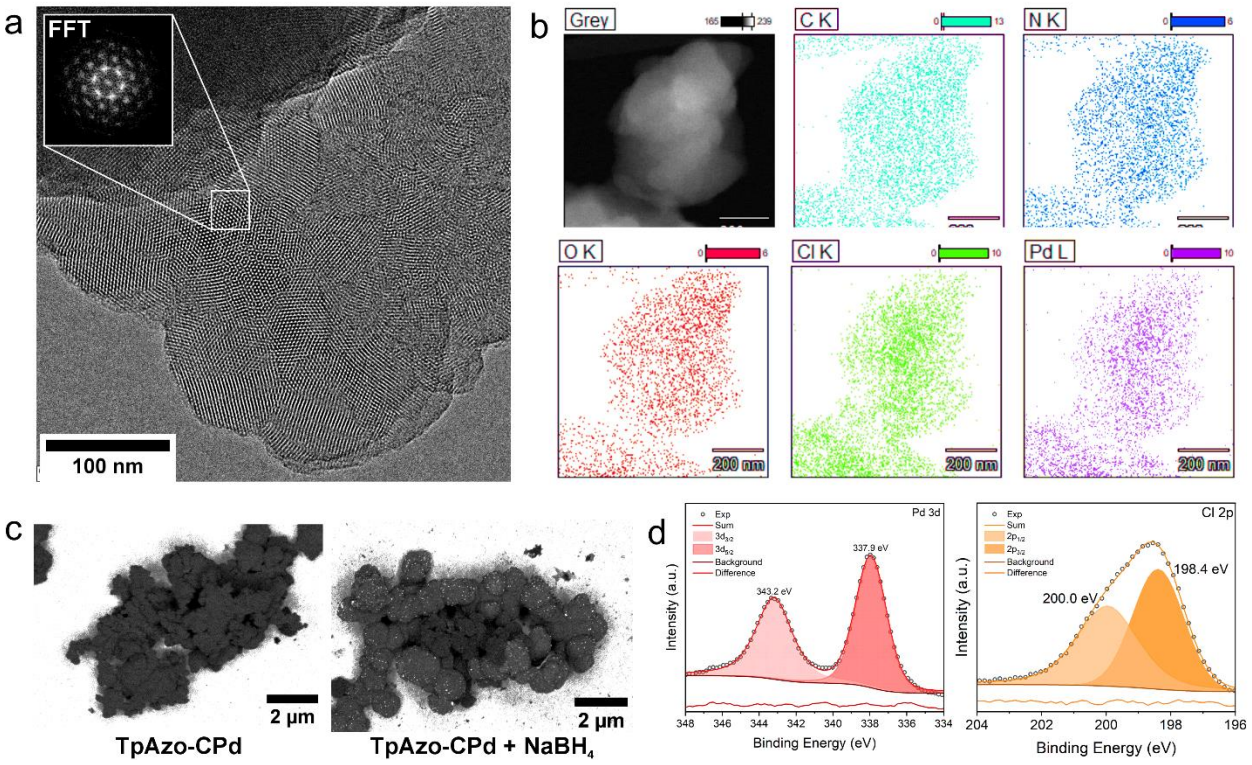

Figure 5. Characterization of isolated palladium atoms in TpAzo-CPd COF. a) HR-TEM image and FFT of a selected area. b) STEM-EDX elemental mapping analysis of the area shown at the top left. c) SEM images using ESB/SE2 detectors. d) Pd 3*d* and Cl 2*p* XPS spectra.

Photocatalytic H_2O_2 production

The photocatalytic activity of TpAzo COFs under NIR light (LED of 810 nm) was evaluated through the generation of H_2O_2 via the reduction of molecular oxygen in a $2e^-$ process (Figure 6a). To investigate the thermodynamic ability of these COFs to reduce oxygen, the energy levels of the highest occupied molecular orbital (HOMO)/ valence band maximum (VBM) and the lowest unoccupied molecular orbital (LUMO) / conduction band minimum (CBM) were determined by electrochemical cyclic voltammetry (Figure S47-S52). The three COFs show similar HOMO values

(approximately 1.2 V vs. NHE pH 7). However, different LUMO energy levels are obtained for TpAzo, TpAzo-Pd, TpAzo-CPd, located at -0.9 V, -0.6 V and -0.5 V vs. NHE pH 7, respectively (Figure 6b). We propose that the significant change in LUMO energy level is induced by palladium coordination to the azo group, perturbing the electronic structure of the N=N bond, the latter showing a major contribution to the LUMO orbital due to its electron-accepting nature.[40] Nevertheless, the LUMO levels of all COFs thermodynamically satisfy the requirement of photocatalytic oxygen reduction via both a two-step superoxide radical pathway and via a one-step two-electron transfer process (Figure 6b).[41]

The photocatalytic production of H_2O_2 by TpAzo COFs was measured with an 810 nm LED using a constant oxygen flow of 100 mL min^{-1}, benzyl alcohol as sacrificial electron donor and the photocatalyst amount was optimized to 4 mg for our setup (Figure S55). As shown in the 10-hour continuous tests (Figure 6c), TpAzo-CPd COF exhibits an evidently higher H_2O_2 production rate of 652.2 μmol g^{-1} h^{-1}, compared to TpAzo-Pd COF (178.7 μmol g^{-1} h^{-1}) and pristine TpAzo COF (119.5 μmol g^{-1} h^{-1}) (all rates were calculated from the first 2 hours of illumination). To verify whether H_2O_2 is produced by photogenerated charges, we measured the H_2O_2 production rate for 4 hours in the dark before switching on the illumination (Figure S56). While 2.6 μmol of H_2O_2 is detected during the first hour for TpAzo-CPd under dark conditions, H_2O_2 production ceased thereafter. The H_2O_2 formed in the dark is likely attributable to the incipient self-oxidation of the TpAzo-CPd COF by the purged oxygen, since no H_2O_2 is detected under Ar (Figure 6d) and obtaining H_2O_2 via self-oxidation has been reported in other studies on molecular photocatalysts for H_2O_2 production.[42] It is noted that the FT-IR spectrum of TpAzo-CPd after a 10-hour continuous illumination test remains identical with the pristine TpAzo-CPd (Figure S57). Apart from some photo-induced Pd reduction (up to 18%) after 10-

hour irradiation (Figure S58), no chemical structure changes have been observed as a consequence of self-oxidation. After switching on the illumination, a continuous 4-hour H_2O_2 production with a rate of 551.9 μmol g^{-1} h^{-1} is observed, consistent with the H_2O_2 production rate obtained from Figure 6c, thus confirming that photogenerated charges of TpAzo-CPd COF are consumed to produce H_2O_2. Excluding the small amounts of hydrogen peroxide produced in the dark, the apparent quantum yield (AQY) of TpAzo-CPd at 810 nm was determined to be 2.2% (Table S3).

To further understand the role of TpAzo-CPd COF for the NIR photocatalytic H_2O_2 production, several other control experiments were carried out. Firstly, we have verified that although Pd nanoparticles can integrate NIR light absorption with catalytic properties, the cyclopalladation complex exhibits superior performance in terms of NIR photocatalytic H_2O_2 production compared to Pd nanoparticles. As shown in Figure 6d, only 65.8 μmol g^{-1} h^{-1} of H_2O_2 was obtained with TpAzo-CPd + $NaBH_4$, wherein the cyclopalladation complex has been disassembled into Pd nanoparticles as demonstrated in Figure 4c. Additionally, reducing the Pd loading amount in TpAzo-CPd also leads to decreased light absorption at 810 nm (Figure 6e). At a Pd loading of 1.4 wt%, the light absorption at 810 nm is nearly identical to that of TpAzo, and the H_2O_2 production rate of this sample under 810 nm illumination becomes negligible (Figure 6f and Figure S56). These findings underscore the critical role of extended light absorption on photocatalytic H_2O_2 production as cyclopalladation of the COF proceeds (Figure 6f).

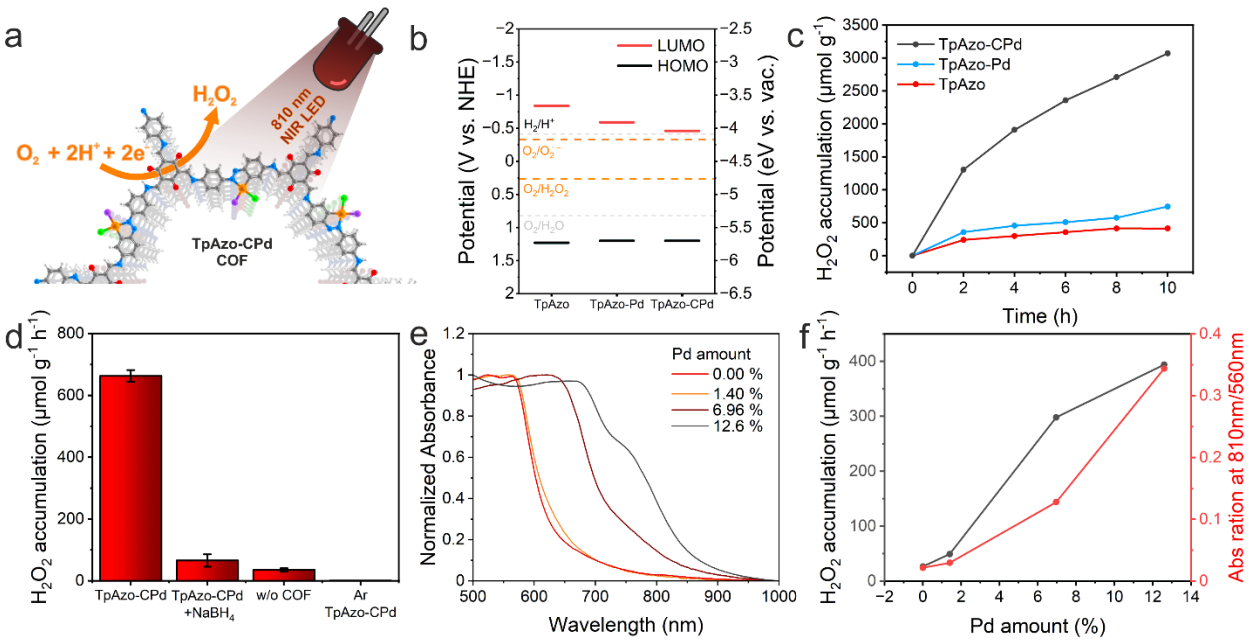

Figure 6. a) Schematic representation of H_2O_2 production *via* a $2e^-$ oxygen reduction reaction under 810 nm LED. In gray, carbon atoms; white, hydrogen; red, oxygen; blue, nitrogen; orange, palladium; green, chlorine; purple, exchangeable ligands. b) Energy levels of the COFs *vs*. vacuum and vs. Normal Hydrogen Electrode (NHE). Reference water splitting potentials (light grey) are defined at pH 7. c) Photocatalytic production of H_2O_2 under 810 nm LED irradiation. d) Control experiments on H_2O_2 production after 2 h of illumination without subtracting the H_2O_2 production obtained from the self-oxidation of the COFs. e) Vis-NIR absorbance spectra from diffuse reflectance spectroscopy of TpAzo-CPd COF with different Pd amounts. f) H_2O_2 production from a series of TpAzo-CPd COFs with different amount of Pd (after extracting the produced H_2O_2 by self-oxidation of the COFs in Figure S53) and relative absorbance at 810 nm of TpAzo-CP COFs with different Pd amounts.

Conclusions

In summary, we have developed a novel post-synthetic functionalization scheme by incorporating a palladacycle in the azobenzene COF backbone by a quantitative cyclopalladation reaction. The resulting COF, TpAzo-CPd, successfully extends

light absorption into the NIR spectrum region and enables the first demonstration of NIR photocatalysis in the field of COFs. Structural characterizations, including solid-state NMR and Raman spectroscopy, etc., establish that the cyclopalladation complex is obtained using methanol as the reaction solvent, whereas acetonitrile only facilitates unspecific N-Pd coordination without the formation of a C-Pd bond. The cyclopalladated COF (TpAzo-CPd) retains the crystallinity of TpAzo and exhibits a uniform distribution of palladacycles in the frameworks without noticeable formation of Pd nanoparticles. Under 810 nm LED illumination, TpAzo-CPd is capable of producing H_2O_2 via photocatalytic oxygen reduction. Further investigations confirm that the NIR light absorption induced by cyclopalladation contributes photogenerated charges crucial for photocatalytic H_2O_2 production. Therefore, this work not only expands the scope of post-synthetic functionalization of COFs by introducing cyclopalladation to the toolbox, but also demonstrates the potential of COFs in NIR photocatalysis. We anticipate that our results will stimulate further discovery of NIR-responsive COFs and advance their applications in harvesting NIR light for photocatalysis for fuel generation, chemical synthesis, and biomedical applications.

Data availability

All data that support the findings of this study are available in the supporting information of this article.

Acknowledgments

Financial support by the Deutsche Forschungsgemeinschaft (DFG, German Research Foundation)— Projektnummer TRR 247-388390466 (project A09, S project), Projektnummer 358283783 – SFB 1333/2 2022 (A03), the DFG under Germany's Excellence Strategy—EXC 2033-390677874—RESOLV, the DFG

cluster of excellence “e-conversion” —EXC 2089/1–390776260, the Max Planck Society, Max Planck Fellowship Programme, the Center for NanoScience, and the Bavarian Research Network SolTech for funding is gratefully acknowledged. The authors thank Eng. Armin Schulz (FKF-MPI) for performing the Raman measurements. Dr. Vesna Srot and Eng. Kersten Hahn (MPI-FKF) for the STEM experiments. The authors acknowledge DESY (beamline P02.1, Hamburg, Germany), a member of the Helmholtz Association HGF, for the provision of experimental facilities. N.G. thanks the Spanish Ministry of Science & Innovation for the “Ramon y Cajal” Program (RYC2018-023888-I) and the funding through PID2021-128805NA-I00. This project has also received funding from the European Research Council (ERC) under the European Union’s Horizon 2020 research and innovation programme (grant agreement No.948829).

Competing interests

The authors declare no competing interests.

TOC

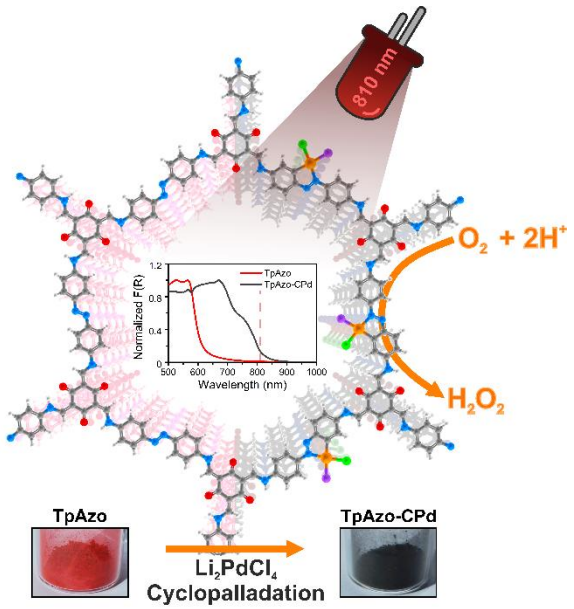

References:

1. Côté Adrien P, Benin Annabelle I, Ockwig Nathan W, O'Keeffe M, Matzger Adam J, Yaghi Omar M. Porous, Crystalline, Covalent Organic Frameworks. *Science* 2005, **310**(5751)**:** 1166-1170.

2. Lyu H, Li H, Hanikel N, Wang K, Yaghi OM. Covalent Organic Frameworks for Carbon Dioxide Capture from Air. *Journal of the American Chemical Society* 2022, **144**(28)**:** 12989-12995.

3. Wang X, Liu H, Zhang J, Chen S. Covalent organic frameworks (COFs): a promising CO2 capture candidate material. *Polymer Chemistry* 2023, **14**(12)**:** 1293-1317.

4. Xue R, Liu Y-S, Huang S-L, Yang G-Y. Recent Progress of Covalent Organic Frameworks Applied in Electrochemical Sensors. *ACS Sensors* 2023, **8**(6)**:** 2124-2148.

5. Grunenberg L, Savasci G, Emmerling ST, Heck F, Bette S, Cima Bergesch A*, et al.* Postsynthetic Transformation of Imine- into Nitrone-Linked Covalent Organic Frameworks for Atmospheric Water Harvesting at Decreased Humidity. *Journal of the American Chemical Society* 2023, **145**(24)**:** 13241-13248.

6. Nguyen HL. Covalent Organic Frameworks for Atmospheric Water Harvesting. *Advanced Materials* 2023, **35**(17)**:** 2300018.

7. Sridhar V, Yildiz E, Rodríguez-Camargo A, Lyu X, Yao L, Wrede P*, et al.* Designing Covalent Organic Framework-Based Light-Driven Microswimmers toward Therapeutic Applications. *Advanced Materials* 2023, **35**(25)**:** 2301126.

8. Ghosh P, Banerjee P. Drug delivery using biocompatible covalent organic frameworks (COFs) towards a therapeutic approach. *Chemical Communications* 2023, **59**(84)**:** 12527-12547.

9. Stegbauer L, Schwinghammer K, Lotsch BV. A hydrazone-based covalent organic framework for photocatalytic hydrogen production. *Chemical Science* 2014, **5**(7)**:** 2789-2793.

10. Rath BB, Krause S, Lotsch BV. Active Site Engineering in Reticular Covalent Organic Frameworks for Photocatalytic CO2 Reduction. *Advanced Functional Materials* 2023, **n/a**(n/a)**:** 2309060.

11. Lin G, Ding H, Chen R, Peng Z, Wang B, Wang C. 3D Porphyrin-Based Covalent Organic Frameworks. *Journal of the American Chemical Society* 2017, **139**(25)**:** 8705-8709.

12. Xiao G, Li W, Chen T, Hu W-B, Yang H, Liu YA*, et al.* Application of Electron-Rich Covalent Organic Frameworks COF-JLU25 for Photocatalytic Aerobic Oxidative Hydroxylation of Arylboronic Acids to Phenols. *European Journal of Organic Chemistry* 2021, **2021**(29)**:** 3986-3991.

13. Li B, Hu Y, Shen Z, Ji Z, Yao L, Zhang S*, et al.* Photocatalysis Driven by Near-Infrared Light: Materials Design and Engineering for Environmentally Friendly Photoreactions. *ACS ES&T Engineering* 2021, **1**(6)**:** 947-964.

14. Bessinger D, Ascherl L, Auras F, Bein T. Spectrally Switchable Photodetection with Near-Infrared-Absorbing Covalent Organic Frameworks. *Journal of the American Chemical Society* 2017, **139**(34)**:** 12035-12042.

15. Xia Y, Zhang W, Yang S, Wang L, Yu G. Research Progress in Donor−Acceptor Type Covalent Organic Frameworks. *Advanced Materials* 2023, **35**(48)**:** 2301190.

16. Segura JL, Royuela S, Mar Ramos M. Post-synthetic modification of covalent organic frameworks. *Chemical Society Reviews* 2019, **48**(14)**:** 3903-3945.

17. Cope AC, Siekman RW. Formation of Covalent Bonds from Platinum or Palladium to Carbon by Direct Substitution. *Journal of the American Chemical Society* 1965, **87**(14)**:** 3272-3273.

18. Nguyen THL, Gigant N, Joseph D. Advances in Direct Metal-Catalyzed Functionalization of Azobenzenes. *ACS Catalysis* 2018, **8**(2)**:** 1546-1579.

19. Dupont J, Consorti CS, Spencer J. The Potential of Palladacycles: More Than Just Precatalysts. *Chemical Reviews* 2005, **105**(6)**:** 2527-2572.

20. Ding S-Y, Gao J, Wang Q, Zhang Y, Song W-G, Su C-Y*, et al.* Construction of Covalent Organic Framework for Catalysis: Pd/COF-LZU1 in Suzuki–Miyaura Coupling Reaction. *Journal of the American Chemical Society* 2011, **133**(49)**:** 19816-19822.

21. Lin S, Hou Y, Deng X, Wang H, Sun S, Zhang X. A triazine-based covalent organic framework/palladium hybrid for one-pot silicon-based cross-coupling of silanes and aryl iodides. *RSC Advances* 2015, **5**(51)**:** 41017-41024.

22. Liu J, Zhan H, Wang N, Song Y, Wang C, Wang X*, et al.* Palladium Nanoparticles on Covalent Organic Framework Supports as Catalysts for Suzuki–Miyaura Cross-Coupling Reactions. *ACS Applied Nano Materials* 2021, **4**(6)**:** 6239-6249.

23. Wang R, Kong W, Zhou T, Wang C, Guo J. Organobase modulated synthesis of high-quality β-ketoenamine-linked covalent organic frameworks. *Chemical Communications* 2021, **57**(3)**:** 331-334.

24. Chandra S, Kundu T, Kandambeth S, BabaRao R, Marathe Y, Kunjir SM*, et al.* Phosphoric Acid Loaded Azo (−N═N−) Based Covalent Organic Framework for Proton Conduction. *Journal of the American Chemical Society* 2014, **136**(18)**:** 6570-6573.

25. Sing KSW. Reporting physisorption data for gas/solid systems with special reference to the determination of surface area and porosity (Recommendations 1984). 1985, **57**(4)**:** 603-619.

26. Ćurić M, Babić D, Višnjevac A, Molčanov K. Simple Route to the Doubly ortho-Palladated Azobenzenes: Building Blocks for Organometallic Polymers and Metallomesogens. *Inorganic Chemistry* 2005, **44**(17)**:** 5975-5977.

27. Nikolaeva MV, Bogdanova EK, Puzyk MV. Azobenzene palladium(II) complexes with β-diketones. *Russian Journal of General Chemistry* 2017, **87**(3)**:** 485-488.

28. Bjelopetrović A, Lukin S, Halasz I, Užarević K, Đilović I, Barišić D*, et al.* Mechanism of Mechanochemical C−H Bond Activation in an Azobenzene Substrate by PdII Catalysts. *Chemistry – A European Journal* 2018, **24**(42)**:** 10672-10682.

29. Bjelopetrović A, Barišić D, Duvnjak Z, Džajić I, Juribašić Kulcsár M, Halasz I*, et al.* A Detailed Kinetico-Mechanistic Investigation on the Palladium C–H Bond Activation in Azobenzenes and Their Monopalladated Derivatives. *Inorganic Chemistry* 2020, **59**(23)**:** 17123-17133.

30. Gutmann V. Principles of Coordination Chemistry in Non-Aqueous Solutions. In: Gutmann V (ed). *Coordination Chemistry in Non-Aqueous Solutions*. Springer Vienna: Vienna, 1968, pp 12-34.

31. Chakraborty I, Carrington SJ, Mascharak PK. Design Strategies To Improve the Sensitivity of Photoactive Metal Carbonyl Complexes (photoCORMs) to Visible Light and Their Potential as CO-Donors to Biological Targets. *Accounts of Chemical Research* 2014, **47**(8)**:** 2603-2611.

32. Maestri M, Balzani V, Deuschel-Cornioley C, Zelewsky AV. Photochemistry and Luminescence of Cyclometallated Complexes. *Advances in Photochemistry*, 1992, pp 1-68.

33. Yang J, Acharjya A, Ye M-Y, Rabeah J, Li S, Kochovski Z*, et al.* Protonated Imine-Linked Covalent Organic Frameworks for Photocatalytic Hydrogen Evolution. *Angewandte Chemie International Edition* 2021, **60**(36)**:** 19797-19803.

34. Terban MW, Ghose SK, Plonka AM, Troya D, Juhás P, Dinnebier RE*, et al.* Atomic resolution tracking of nerve-agent simulant decomposition and host metal–organic framework response in real space. *Communications Chemistry* 2021, **4**(1)**:** 2.

35. Copeman C, Bicalho HA, Terban MW, Troya D, Etter M, Frattini PL*, et al.* Adsorptive removal of iodate oxyanions from water using a Zr-based metal–organic framework. *Chemical Communications* 2023, **59**(21)**:** 3071-3074.

36. Terban MW, Billinge SJL. Structural Analysis of Molecular Materials Using the Pair Distribution Function. *Chemical Reviews* 2022, **122**(1)**:** 1208-1272.

37. Chu C, Huang D, Gupta S, Weon S, Niu J, Stavitski E*, et al.* Neighboring Pd single atoms surpass isolated single atoms for selective hydrodehalogenation catalysis. *Nature Communications* 2021, **12**(1)**:** 5179.

38. Muravev V, Spezzati G, Su Y-Q, Parastaev A, Chiang F-K, Longo A*, et al.* Interface dynamics of Pd–CeO2 single-atom catalysts during CO oxidation. *Nature Catalysis* 2021, **4**(6)**:** 469-478.

39. Militello MC, Simko SJ. Palladium Chloride (PdCl2) by XPS. *Surface Science Spectra* 1994, **3**(4)**:** 402-409.

40. Wu H, He X, Du X, Wang D, Li W, Chen H*, et al.* The Linkage-Moderated Covalent Organic Frameworks with □C=N□ and □N□N□ on Charge Transfer Kinetics Towards the Robust Photocatalytic Hydrogen Activity. *Small* 2023, **19**(48)**:** 2304367.

41. Freese T, Meijer JT, Feringa BL, Beil SB. An organic perspective on photocatalytic production of hydrogen peroxide. *Nature Catalysis* 2023, **6**(7)**:** 553-558.

42. Yang H, Li C, Liu T, Fellowes T, Chong SY, Catalano L*, et al.* Packing-induced selectivity switching in molecular nanoparticle photocatalysts for hydrogen and hydrogen peroxide production. *Nature Nanotechnology* 2023, **18**(3)**:** 307-315.